Interferometric approaches to atom-surface van der Waals interactions in atomic mirrors

Michel Gorlicki, Sylvain Feron, Vincent Lorent, and Martial Ducloy
Laboratoire de Physique des Lasers, UMR 7538 du CNRS, Institut Galilée, Université Paris Nord, Avenue J. B. Clément, F-93430 Villetaneuse, France

(Received 12 July 1999; published 9 December 1999)

We analyze the possibilities of approaching atom-surface interactions through their contribution to the atomic matter de Broglie wave phase, in an interferometer based on an evanescent light atomic mirror. The surface interactions produce an additional phase shift that is evaluated to a few times π for a neon atom in a metastable state. We propose and investigate an experimental procedure that uses the principles of polarization (for instance, Stern-Gerlach) interferometers in order to monitor these long-range interactions (van der Waals, Casimir-Polder, etc.) between a ground-state or metastable-state atom and either a metallic or a dielectric surface. Our approach gives access to the differential phase shift between Zeeman sublevels, and should then be sensitive to an eventual anisotropy of the atom-surface interaction.

PACS number(s): 03.75.Be, 39.20.+q, 34.50.Dy

I. INTRODUCTION

Atom-surface interactions have been given a great deal of attention for decades, and investigated in several fields of physics. First theoretical considerations may be found, through different approaches, in the pioneering studies of Lennard-Jones [1], Casimir and Polder [2], and Lifschitz [3]. It is now classical to represent the ''long-range interaction'' (i.e., distances larger than 1 nm) in terms of an interaction between the atom considered as a fluctuating electrical dipole and its image within the material limited in space by the surface. In a pure electrostatic study, this description gives rise to an *attractive* interaction whose amplitude variation is proportional to y^{-3}, where y is the transverse distance from the atom to the surface [3]; atom-surface interactions exhibiting this kind of behavior were referred to as van der Waals forces. More accurate theories, taking into account the electromagnetic propagation, were carried out over the years, resulting in more complex variation laws, including the Casimir-Polder effect [2], whose signature is a y^{-4} variation at large distances ($\geqslant$100 nm) (for a review, see [4]).

Considering the effect of the surface on internal properties of atoms, early studies were performed by Drexhage *et al.*, addressing the influence on the spontaneous-emission rate in a pure electromagnetic approach [5]. Using either classical or quantum-mechanical analysis, various aspects of the modifications of the *inner state* of an atom induced by the presence of the surface were extensively studied [6,7] and are still under consideration. Effects on the ground state as well as excited state were described, from which, in return, better quantitative evaluations of the mechanical effect were given. QED treatments were achieved for alkali-metal atoms, which gave back the previously obtained results as limiting cases [7]. The amazing possibility of an overall repulsive interaction in specific conditions, initially mentioned in [8], was described in a full quantum-mechanical treatment of both the atom state and the resonance spectrum of the surface [9], and observed recently [10].

Most early experimental studies of the *mechanical* interaction relied upon observations of the trajectory deflections produced by these forces, using various experimental configurations [11–13]. More recently, the mechanical attraction, combined to a repulsive optical potential in an atomic mirror, was successfully monitored through the threshold effect resulting from the two interactions competition [14]. Since the van der Waals interaction produces a shift of the eigenvalues of the atom, various types of *spectroscopic* studies were also developed. Selective reflection methods can access, through linear as well as nonlinear spectroscopy schemes, the specific response of atoms coming close to a wall in a cell, and have been extensively used to monitor the shifts induced both in fundamental and excited levels [15,16]. A beam of atoms flowing in the very middle of a planar microcavity, where the opposite mechanical van der Waals forces compensate, was successfully used to measure by spectroscopic ways the y^{-3} dependence of the level shifts with alkali-metal atoms [17].

The present paper presents a theoretical study of the phase effect of long-distance atom-surface interactions in an atomic interferometry scheme. As any interaction, van der Waals forces produce an additional phase to the de Broglie wave associated to the overall motion of the atom [14,18]. Obtaining a quantitative interferometric evaluation of the influence of this phase is the purpose of this paper. The interferometer under study is an atomic mirror [19,20], in which incoming atoms are reflected by an evanescent wave supported by the studied surface. We consider atoms in the thermal velocities range, with a grazing incidence (a few mrad), as seen in Fig. 1. These atoms are prepared in a coherent superposition of internal states, namely Zeeman substates, using methods of polarization interferometry [21]. Since the optical potentials experienced by atoms being in each Zeeman state are different, they are, respectively, associated to different motions in the transverse direction (y); recombination of the paths at the output makes up an atomic interferometer. A first point is that the van der Waals phases are then different along the Zeeman paths, and the resulting interferometric state of the de Broglie wave at the output is sensitive to them. A second and major point lies in a remarkable feature of the evanescent potential. As will be seen in Sec. II, the ratio between

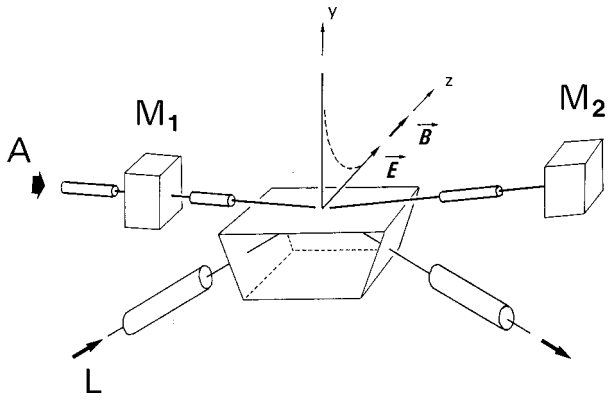

FIG. 1. Principle of the interferometer. At arrow *A*, atoms are coming at a grazing incidence with respect to a plane surface, and are reflected by the atom mirror optical potential created by an evanescent wave supported by the surface, which may be produced by a laser wave (*L*) in total internal reflection [14,20]. M_1 is the first separatrix, in which atoms are prepared in a specific linear combination of Zeeman substates, using schemes relying on optical pumping or Majorana mixing [21,26]. M_2 stands for the output separatrix, which merges the outgoing paths to produce interferences.

the phases due to the atomic mirror itself (i.e., the interaction with the evanescent wave) for two different paths is independent of the amplitude of the electric field. This provides a convenient phase reference for the study of van der Waals contribution to the phases. A third point is concerned with the magnetic field. The van der Waals phase along a Zeeman substate path is dispersive, and velocity averaging in an actual experiment could wash out the resulting fringes. We thus consider an atomic mirror merged in an adjustable homogeneous static magnetic field, which adds an additional phase, whose dispersion law is different. This will be seen as providing a compensation to velocity dispersion, allowing observation of fringes for relatively wide velocity distributions.

In Sec. II, the framework of the study is presented and the assumptions of the model are stated. The various contributions to the de Broglie phase along the different paths in the interferometer are computed in Sec. III, and Sec. IV then gives the signal expected in an actual interferometry experiment. A discussion of the theoretical predictions, as well as the range of application of this work, is given in Sec. V.

II. ATOMIC MIRROR DESCRIPTION

The atomic mirror is produced by an evanescent wave (in the $o\vec{y}$ direction), running along a direction parallel to the surface of a dielectric plane. The frequency of the wave ω_L is quasiresonant with a transition $|g\rangle \leftrightarrow |e\rangle$ of the atom, where $|g\rangle$ is a long life level (ground state or metastable), and $|e\rangle$ an exited level, with a lifetime γ_e; however, the (blue) detuning $\Delta\omega = \omega_L - \omega_{eg}$ will always be large enough ($\Delta\omega \gg \gamma_e$) so that γ_e may be neglected. Level $|g\rangle$ ($|e\rangle$) is characterized by a total angular momentum F_g (F_e) and consists of a set of $2F_g+1$ ($2F_e+1$) Zeeman substrates. The mirror is merged into a static magnetic field $\vec{B}$, whose *direction remains homogeneous* and will be taken as the quantification axis $o\vec{z}$:$\vec{B}=\overline{B}o\vec{z}$.

Under assumptions that will be examined hereafter, together with the relevant definitions, the total evolution for an atom initially in the multiplicity $\{|g,m\rangle\}$ may be described with the simplified Hamiltonian,

$$\mathcal{H}_{\rm eff}=\sum_m \left[\frac{P_y^2}{2M_{\rm at}}+\xi_m^2\frac{\hbar\Omega_R^2(Y)}{4\Delta}-\frac{\hbar C_g}{Y^3}\right]\otimes|g,m\rangle\langle g,m| + \left[\frac{P_x^2+P_z^2}{2M_{\rm at}}-m\hbar\omega_B^g(X,Z)\right]\otimes|g,m\rangle\langle g,m|. \quad (2.1)$$

To reach Eq. (2.1), we proceed in four stages.

A. Zeeman interaction

The linear Zeeman interaction with the magnetic field $\vec{B}$, when taking its constant direction along the quantification axis $o\overline{z}$, is diagonal and given by

$$V_B=-\hbar\sum_{m,m'} m\omega_B^g(X,Z)|g,m\rangle\langle g,m| + m'\omega_B^e(X,Z)|e,m'\rangle\langle e,m'|, \quad (2.2)$$

where $\omega_B^g=g_g\mu_B\overline{B}/\hbar$ is the Larmor frequency within level $|g\rangle$ (ω_B^e for $|e\rangle$). As appears in Eq. (2.2), we suppose that $\overline{B}$ does not vary along the transverse direction $o\vec{y}$.

B. Interaction with the evanescent light

We consider an electric dipole interaction $V_{\rm opt}(\vec{R}) = -\vec{D}\cdot\vec{E}(\vec{R})$, the electric field being given by

$$\vec{E}(\vec{R})=\tfrac{1}{2}(\vec{\mathcal{E}}e^{-\kappa_{\rm opt}Y}e^{i(\vec{k}_{\rm opt}\cdot\vec{R}-\omega_L t)}+\text{c.c.}), \quad (2.3)$$

where $\vec{k}_{\rm opt}$ refers to a propagation parallel to the dielectric surface. In Eq. (2.3), $\vec{R}$ is an *operator* describing the position of the atom. However, for a coherent electromagnetic wave, it is usual to replace it by a *classical* $\vec{r}=\vec{v}t$, where $\vec{v}$ corresponds to an initial velocity of the atom (to be examined later on). One accounts this way for the first-order Doppler shift $\Delta_D=\vec{k}_{\rm opt}\cdot\vec{v}$.

We assume that the *laser polarization* $\vec{\mathcal{E}}$ *is principal* with respect to the quantization direction. The simplest case occurs with a linear polarization and $\vec{\mathcal{E}}\|\vec{B}$, while some more complex schemes may be found for specific F and F' values [30]. As a consequence of this assumption, a given state $|g,m\rangle$ in the lower level is only coupled by the dipole interaction to *one* state $|e,m'\rangle$ in the upper level (m' depending on the polarization).

Under the rotating-wave approximation (RWA), the interaction may be written in the rotating frame:

$$V_{\rm opt}(Y) = -\hbar \sum_m \frac{\xi_m \Omega_R(Y)}{2} \otimes |g,m\rangle\langle e,m'| + \text{c.c.}, \tag{2.4}$$

where $\Omega_R(Y) = \hbar^{-1}\langle g\|\vec{D}\|e\rangle \cdot \vec{\mathcal{E}} e^{-\kappa_{\rm opt} Y}$ is the Rabi frequency and ξ_m is the relevant Clebsch-Gordan coefficient. In addition, the internal part of the Hamiltonian simply becomes

$$\mathcal{H}_0 = -\hbar \sum_{m'} \Delta |e,m'\rangle\langle e,m'|, \tag{2.5}$$

where $\Delta \equiv \Delta\omega - \Delta_D$.

C. Van der Waals interaction

The van der Waals interaction considered here is a long-range surface interaction (typically $y > 1$ nm), which can be described, for a perfect metallic surface, by a Hamiltonian of the form [4]

$$V_{\rm VdW} = -\frac{\overline{D}^2 + D_y^2}{16 Y^3}, \tag{2.6}$$

where Y is the operator associated to the transverse distance to the surface, and $\overline{D}$ is the electric dipole; for a dielectric surface, Eq. (2.6) must be reduced by a factor $(\epsilon - 1)/(\epsilon + 1)$ [3,6], where ϵ is the electric permittivity. In the general case, evaluation of Eq. (2.6) involves many intermediate states of the atom, and will induce coupling between different levels. This anisotropy may be responsible, for instance, for a decay of some metastable levels or transitions between selected states [22]; however, such effects need still to be given experimental evidence. For the sake of simplicity, we consider at this stage a *scalar* van der Waals interaction, which results in a diagonal interaction term,

$$V_{\rm VdW}(Y) = -\hbar \sum_{m,m'} \left[\frac{C_g}{Y^3} \otimes |g,m\rangle\langle g,m| + \frac{C_e}{Y^3} \otimes |e,m'\rangle\langle e,m'| \right], \tag{2.7}$$

where $\hbar C_g$ accounts for the strength of the interaction for the multiplicity $|g\rangle$ ($\hbar C_e$ for $|e\rangle$). The case of more complex van der Waals effects will be outlined later on.

D. Adiabatic following

Setting apart the dynamical terms, the Hamiltonian that results from the preceding assumptions may now be written as the sum of *independent* two-state systems, each one corresponding to a single value of m in level $|g\rangle$ (or equivalently a value of m' in $|e\rangle$),

$$V(\vec{R}) = \sum_m V_m(X,Y,Z) \tag{2.8}$$

with

$$\frac{V_m(X,Y,Z)}{\hbar} = -\Delta |e,m'\rangle\langle e,m'| - \frac{\xi_m \Omega_R(Y)}{2} \otimes |g,m\rangle\langle e,m'| + \text{c.c.} - \sum_{f\mu = gm, em'} \left\{ \mu \omega_B^f(X,Z) + \frac{C_f}{Y^3} \right\} \otimes |f,\mu\rangle\langle f,\mu|. \tag{2.9}$$

Projecting onto the basis $\{|g,m,\overline{r}\rangle, |e,m',\vec{r}\rangle\}$, Eq. (2.9) is then easily diagonalized, giving straightforward expressions for the eigenvalues $U_{\pm}^m(\vec{r})$ [18]. We assume that the *atom will undergo an adiabatic following* along the adiabatic channels. This model is classical for atomic mirrors, and is usually justified for large detunings. When van der Waals interactions are taken into account, it implies that the atom will not explore a region which is too close to the surface. Moreover, we suppose here that the detuning is larger than any other term present in Eq. (2.9):

$$\frac{\Omega_R(y)}{\Delta} \ll 1, \quad \omega_B, \frac{C_g}{y^3} \ll \Delta. \tag{2.10}$$

With conditions (2.10), $U_{\pm}^m(\overline{r})$ may further be developed up to first order. For $U_+^m(\vec{r})$, which connects to the energy of $|g,m,\vec{r}\rangle$ in the asymptotic region ($y \to +\infty$), one gets

$$U_+^m(\vec{r}) = V_+^m(y) - m\hbar\omega_B^g(x,z), \tag{2.11a}$$

where

$$V_+^m(y) = \hbar \frac{\xi_m^2 \Omega_R^2(y)}{4\Delta} - \hbar \frac{C_g}{y^3}. \tag{2.11b}$$

The point is now reached where the evolution of each state, starting asymptotically in any $|g,m\rangle$ or $|e,m'\rangle$, is decoupled. It is then equivalent, for an atom entering the interaction zone in an internal state belonging to $\{|g,m\rangle\}$ (which is the case of the experiments to be considered), to describing the total motion using the effective Hamiltonian (2.1) within this multiplicity.

III. THE PHASES FOR A STATE $|g, m\rangle$

The stationary wave function of an input atom corresponding to a *total energy* E is described by the time-independant Schrödinger equation. The form of the Hamiltonian (2.1) allows a separation between the $o\vec{y}$ and the parallel $(o\vec{x}, o\vec{z})$ directions; if $|\Psi\rangle$ is the total state of the atom, we set $E = E_{\parallel} + E_{y'}$ and

$$\langle g,m,\vec{r}|\Psi\rangle = \chi_m(x,z)\psi_m(y) \tag{3.1}$$

and the equations are

$$\left\{ \frac{d^2}{dy^2} + K_y^2 \left[1 - \frac{V_+^m(y)}{E_y} \right] \right\} \psi_m(y) = 0, \tag{3.2a}$$

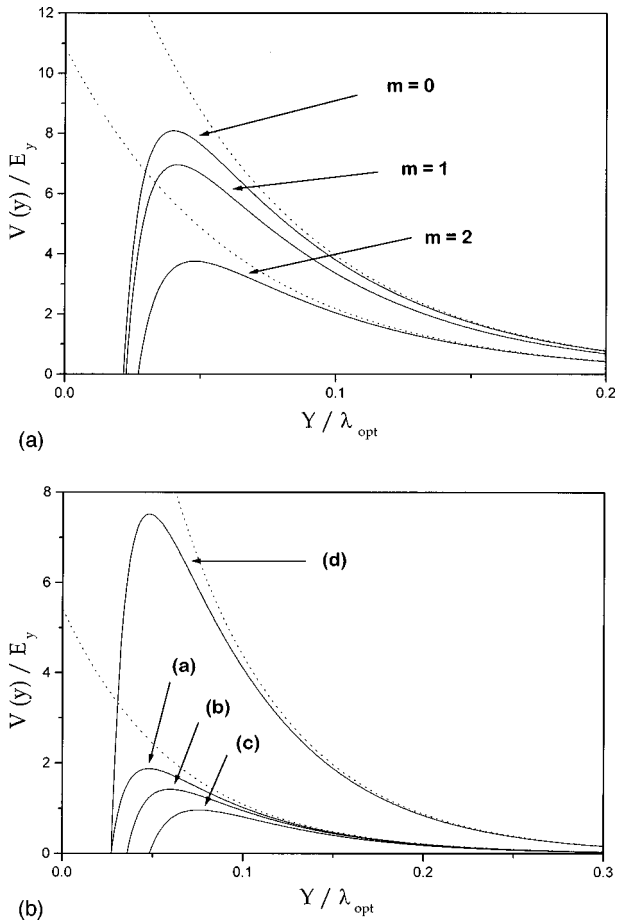

FIG. 2. Interaction potentials for an incoming neon atom in the metastable $1s^5$, $J=2$ level. The evanescent wave is quasiresonant with (a) the $J=2\leftrightarrow J=3$ transition at $\lambda_{opt}=640.2$ nm; (b) the $J=2\leftrightarrow J=2$ transition at $\lambda_{opt}=614.3$ nm. The equivalent Rabi frequency $(2\pi)^{-1}\Omega_R^2(0)/4\Delta$ (referring to a Clebsch-Gordon coefficient equal to 1) is 2 GHz, the range of the evanescent wave is $\kappa_{opt}=\lambda_{opt}/8$ [see Eq. (2.3)]. In (a), the van der Waals strength is $(2\pi)^{-1}C_g=2$ kHz μm^3. In (b), curves *a*, *b*, and *c* correspond to $m=1$, and $(2\pi)^{-1}C_g=1,2,4$ kHz μm^3; curve *d* is the $m=2$ potential, for the latest value. There is no potential for $m=0$. Dotted lines represent the corresponding *optical potentials* alone.

$$\left\{\frac{\partial^2}{\partial x^2}+\frac{\partial^2}{\partial z^2}+K_{\|}^2\left[1+\frac{m\hbar\omega_B^g(x,z)}{E_{\|}}\right]\right\}\chi_m(x,z)=0, \tag{3.2b}$$

where we have defined $K_{y,\|}^2=2M_{at}\hbar^{-2}E_{y,\|}$.

A. Phases induced along $o\vec{y}$

A major assumption of the present calculation is that the variations of $V_+^m(y)$ are smooth enough to ensure the validity of the *semiclassical JWKB approximation* [23]. In Fig. 2, the shapes $V_+^m(y)$ for different m are given in the case of a neon metastable atom, for which atom mirror experiments were performed [20]. When the transverse energy $E_y<V_+^m(y)$ for $y<y_r^m$, the solution of Eq. (3.2a) in the classically permitted region $y_r^m<y$ may then be written as

$$\psi_m(y)=A_m\{\exp[-i\varphi^m(y)]-R_m\exp[+i\varphi^m(y)]\} \tag{3.3}$$

with

$$\varphi^m(y)=K_y\int_{y_r^m}^{y}\left(1-\frac{V_+^m(y')}{E_y}\right)^{1/2}dy', \tag{3.4}$$

where y_r^m is the classical turning point defined by $E_y=V_+^m(y_r^m)$. For E_y far enough below the maximum of $V_+^m(y)$ [24], one gets $R_m=\exp(i\pi/2)$; in the asymptotic region $y\to+\infty$, $V_+^m(y)\to 0$, Eq. (3.3) then becomes

$$\psi_m(y)=A_m e^{-(i/2)\Phi^m}[e^{-iK_y y}-\exp(i\Phi^m)e^{+iK_y y}] \tag{3.5}$$

with

$$\Phi^m=\frac{\pi}{2}+2K_y\int_{y_r^m}^{+\infty}\left[\left(1-\frac{V_+^m(y')}{E_y}\right)^{1/2}-1\right]dy'-K_y y_r^m. \tag{3.6}$$

Phase Φ^m represents the asymptotic dephasing between an incoming and an outgoing plane wave, for a state $|g,m\rangle$, when the phase reference for the motion along $o\vec{y}$ is taken at $y=0$. It cannot be given an analytic expression with $V_+^m(y)$ and must be computed numerically. However, integration can be carried out when considering only the optical potential of the atomic mirror (no van der Waals interaction). Introducing

$$V_{opt}^m(y)=\hbar\,\frac{\xi_m^2\Omega_R^2(0)e^{-2\kappa_{opt}y}}{4\Delta} \tag{3.7}$$

in Eq. (3.6), we find

$$\Phi_{opt}^m=\frac{\pi}{2}-2K_y\mathcal{L}_{opt}^m, \tag{3.8a}$$

where we have defined

$$\mathcal{L}_{opt}^m=\frac{1}{\kappa_{opt}}\left\{1+\tfrac{1}{2}\ln\left[\xi_m^2\frac{\hbar\Omega_R^{eff}}{4}\right]\right\}, \tag{3.8b}$$

in which

$$\Omega_R^{eff}=\frac{\Omega_R^2(0)}{4\Delta}. \tag{3.8c}$$

Figure 3 exhibits the phases Φ^m and Φ_{opt}^m when increasing the Rabi frequency.

A remarkable property results from Eq. (3.8) for the phase difference between two substates $|g,m\rangle$ and $|g,m'\rangle$:

$$\Delta\Phi_{opt}^{mm'}\equiv K_y\mathcal{L}_{opt}^{m,m'}=2\,\frac{K_y}{\kappa_{opt}}\ln\left[\frac{|\xi_m'|}{|\xi_m|}\right]. \tag{3.9}$$

As seen in Eq. (3.9), $\Delta\Phi_{opt}^{mm'}$ does not depend on the strength of the optical potential; this peculiarity is due to the decreas-

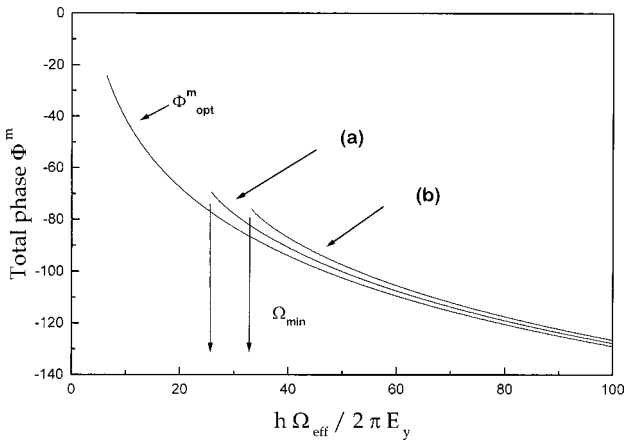

FIG. 3. Variation of the total phase for different values of the van der Waals constant, for neon atoms at 780 m/s, with an incidence angle $\alpha_{in} \approx 2$ mrad. The optical transition is the $J=2 \leftrightarrow J=2$ line at $\lambda_{opt}=614.3$ nm. Evanescence range is $\kappa_{opt}=\lambda_{opt}/8$, equivalent Rabi frequency $(2\pi)^{-1}\Omega_R^2(0)/4\Delta$ is 2 GHz. The phases are shown for the $m=1$ Zeeman sublevel. Curves *a* and *b* correspond to $(2\pi)^{-1}C_g=2$ and 4 kHz μm^3. Ω_{min} points out the minimum values to get reflection.

ing exponential shape of $V_{opt}^m(y)$. A variation of $\Delta\Phi^{mm'}$ versus Ω_R^{eff} can then only be produced by an additional interaction. We define here

$$\Delta\Phi^{m,m'} \equiv \Phi^m - \Phi^{m'} = \Delta\Phi_{opt}^{mm'} + \delta\varphi_{VdW}^m - \delta\varphi_{VdW}^{m'}$$
$$\equiv \Delta\Phi_{opt}^{mm'} + \delta\varphi_{VdW}^{mm'}(\Omega_R^{eff}), \qquad (3.10)$$

where expressions of $\delta\varphi_{VdW}^{m,m'}$ are easily derived from Eqs. (3.6) and (3.9). Figure 4 shows this variation of $\Delta\Phi^{mm'}$, due to the van der Waals interaction considered earlier.

B. Phase induced in the motion parallel to the surface

As the magnetic potential is very small when compared to the energy $E_\parallel$, the motion along the surface may be approximated by a classical path undergone at constant initial velocity $M_{at}^{-1}\hbar\overline{K_\parallel}$. Defining the abscissa ς along this direction, with respect to a reference point (x_0, z_0), Eq. (3.2b) may be rewritten as

$$\left\{\frac{d^2}{d\varsigma^2} + K_\parallel^2\left[1 + \frac{m\hbar\varpi_B(\varsigma)}{E_\parallel}\right]\right\}\chi_m(\varsigma) = 0 \qquad (3.11)$$

with $\varpi_B(\varsigma) \equiv \omega_B^g[\cos\theta(\varsigma-\varsigma_0)+x_0, \sin\theta(\varsigma-\varsigma_0)+z_0]$, where $\varsigma_0 = x_0\cos\theta + z_0\sin\theta$, and $\cos\theta = \vec{K}_\parallel \cdot o\vec{x}/|\vec{K}_\parallel|$. We assume $\hbar\varpi_B \ll E_\parallel$; an approximate solution of Eq. (3.11) corresponding to an initial state propagating in the direction of $\vec{K}_\parallel$ is then

$$\chi_m(\varsigma) = b_m \exp\left[+iK_\parallel \int_{\varsigma_{in}}^{\varsigma_{out}} \left(1 + \frac{m\hbar\varpi_B(\varsigma')}{E_\parallel}\right)^{1/2} d\varsigma'\right], \qquad (3.12)$$

which can be further developed as

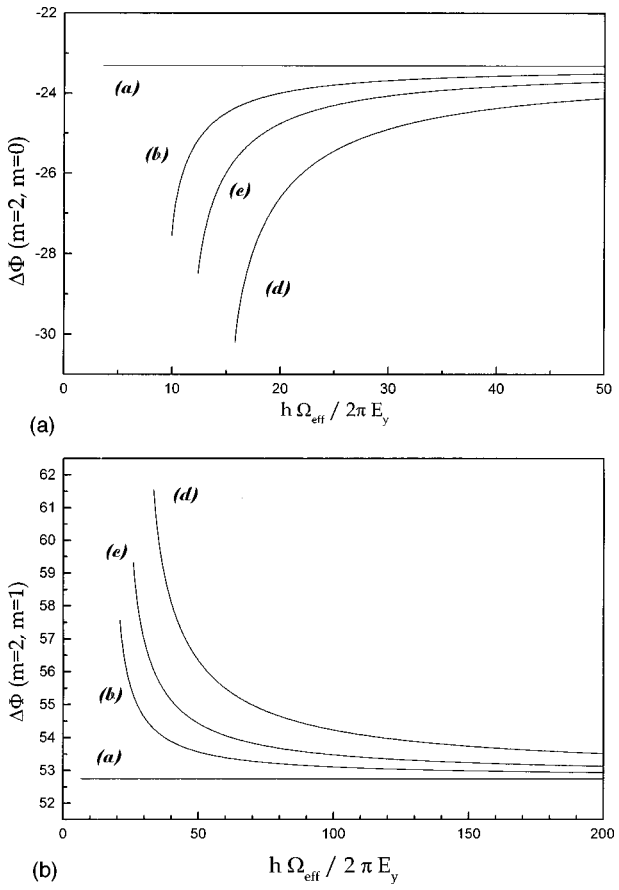

FIG. 4. Examples of phase differences along two Zeeman substrates paths, for (a) transition $J=2 \leftrightarrow J=3$ at $\lambda_{opt}=640.2$ nm; and (b) transition $J=2 \leftrightarrow J=2$ at $\lambda_{opt}=614.3$ nm. Curves *a*, *b*, *c*, and *d*, respectively, correspond to $(2\pi)^{-1}C_g=0$, 1, 2, and 4 kHz μm^3. Other parameters are as in Fig. 3.

$$\chi_m(\varsigma) \cong b_m e^{iK_\parallel(\varsigma_{out}-\varsigma_{in})}\exp(im\Phi_B), \qquad (3.13a)$$

where, using $K_\parallel^2 = 2M_{at}\hbar^{-2}E_\parallel$,

$$\Phi_B = \frac{M_{at}}{\hbar K_\parallel}\int_{\varsigma_{in}}^{\varsigma_{out}} \varpi_B(\varsigma')d\varsigma'. \qquad (3.13b)$$

In the case of a homogeneous field $\overline{B}$, Eq. (3.13b) simply becomes

$$\Phi_B = \frac{M_{at}}{\hbar K_\parallel}\varpi_B(\varsigma_{out}-\varsigma_{in}) \equiv \frac{M_{at}}{\hbar K_\parallel}\varpi_B L, \qquad (3.14)$$

where L is the total distance covered by the atom along the surface.

IV. ATOM INTERFEROMETRY EXPERIMENTS

A. Principle of the experiments

The principle of atom interferometry experiments has been described extensively [21]. Wave interferometry involves at least (i) a separatrix which divides the input wave into two or more coherent subwaves; (ii) different paths

along which the subwaves are to experience different phase stories; (iii) a mixing device, which actually is a second separatrix; and (iv) an analyzer that selects one of the output channels of this last separatrix. Interference patterns are then generated by varying, through an adjustable parameter, the phase differences accumulated along the paths.

In the case of the de Broglie wave of an atom, an additional feature is brought up by the internal structure, which provides supplementary degrees of freedom. For instance, the separatrices may then consist of mixing devices yielding linear combinations of internal states, while the further paths are either spatially separated (as in Ramsey fringe configurations [25]) or not (longitudinal Stern-Gerlach interferometry [26]). Such a scheme can be represented by

$$|\Psi^{\text{final}}\rangle = AM_2S(\text{out}\leftarrow\text{in})M_1[P]|\Psi^{\text{initial}}\rangle, \tag{4.1}$$

where operators M_1 and M_2, respectively, stand for the two separatrices, S is the evolution along the different paths, and A is the analyzer. When the involved states are asymptotically degenerated (such as Zeeman substates), an additional polarizer P is necessary, to make sure that the atom enters the interferometer in a defined state.

The experiment we study relies on the methods of polarization Stern-Gerlach schemes. An atom in the $|g\rangle$ level, with initial velocity $\vec{v}^{\text{in}} = M^{-1}_{\text{at}}\,\hbar\vec{K}^{\text{in}}$, comes in at a grazing incidence characterized by the angle α_{in} from the surface, such as $\alpha_{\text{in}} \ll 1$. The preparation step yields a linear combination of Zeeman states $|g,m\rangle$, where m refers to the direction of the magnetic field $\vec{B}$:

$$M_1[P]|\Psi^{\text{initial}}\rangle \equiv |\Psi^{\text{in}}\rangle = \sum_m c_m|g,m\rangle \otimes |\vec{K}^{\text{in}}\rangle. \tag{4.2}$$

The atomic mirror analyzed in Sec. III is the differential phasing zone; $S(\text{out}\leftarrow\text{in})$ thus reads

$$S(\text{out}\leftarrow\text{in}) = \sum_{m'} e^{i(\Phi^{m'} + m'\Phi_B)}|g,m'\rangle\langle g,m'| \tag{4.3}$$

and the signal observed at the output is proportional to

$$\mathcal{S} = \|\langle\vec{r}|\Psi^{\text{final}}\rangle\|^2$$

$$= \sum_{m,m'} c^*_{m'}c_m\langle g,m'|M_2^\dagger A^\dagger A M_2|g,m\rangle e^{i[\Delta\Phi^{mm'} + (m-m')\Phi_B]}. \tag{4.4}$$

Experimentally, input atoms are characterized by a velocity distribution, both in transverse and longitudinal directions. The transverse distribution depends highly on the experimental collimating conditions, and may be chosen to have no significant influence here (see [27]). The longitudinal velocity distribution is $\rho(v-\overline{v})$, centered around $\overline{v}$ (up to $\overline{v} \approx 1$ km/s for a thermal supersonic beam), with a typical width Δv. As $\alpha_{\text{in}} \ll 1$, we can take it as a distribution of parallel velocities $v_\parallel = M^{-1}_{\text{at}}\,\hbar K_\parallel$. The averaged signal finally measured is

$$I = \int dv_\parallel \rho(v_\parallel - \overline{v})\mathcal{S}(v_\parallel). \tag{4.5}$$

Fringes are then produced when scanning the magnetic-field amplitude $\overline{B}$. The form of operators M_2 and A, as well as the c_m coefficients, depend on the specific polarizing and analyzing devices; examples are outlined further on.

B. The double role of the magnetic field

It follows right from Eq. (4.4) that $\mathcal{S}$ contains a sum of oscillating terms of the form

$$\cos\{\eta^{m_1m_2} + \Delta\Phi^{m_1m_2} + (m_1-m_2)\Phi_B\} \equiv \cos\Gamma(1,2), \tag{4.6}$$

where $\eta^{m_1m_2}$ stands for a possible phase of the coefficients in Eq. (4.4). With Eqs. (3.9), (3.10), and (3.14), $\Gamma(1,2)$ reads

$$\begin{aligned}\Gamma(1,2) &= 2K_y\Delta\mathcal{L}^{1,2}_{\text{opt}} + \delta\varphi^{m_1m_2}_{\text{VdW}}(K_y,\Omega^{\text{eff}}_R) \\ &\quad + \frac{M_{\text{at}}}{\hbar K_\parallel}(m_1-m_2)\varpi_B L + \eta^{m_1m_2} \\ &\cong v_\parallel\frac{2\alpha_{\text{in}}M_{\text{at}}}{\hbar}\Delta\mathcal{L}^{1,2}_{\text{opt}} + \delta\varphi^{m_1m_2}_{\text{VdW}}(v_\parallel,\Omega^{\text{eff}}_R) \\ &\quad + \frac{1}{v_\parallel}(m_1-m_2)\varpi_B L + \eta^{m_1m_2},\end{aligned} \tag{4.7}$$

in which the variations with Ω^{eff}_R result only from the van der Waals interaction. A straightforward way to generate fringes would then consist in scanning the value of Ω^{eff}_R, in the absence of magnetic field ($\varpi_B = 0$). However, due to the velocity distribution, each oscillating term is shaped by an envelope centered at the point of stationary phase versus $v_\parallel$. When $\varpi_B = 0$, this point corresponds to $\Gamma(1,2) = 0$ and cannot be reached [when $\Omega^{\text{eff}}_R \to \infty$, $\Gamma(1,2) \to \Delta\Phi^{m_1m_2}_{\text{opt}} \approx 50\pi$]; whatever the values of Ω^{eff}_R, and for $\Delta v/\overline{v} \geqslant 1\%$, the fringes are washed out. In contrast, when $\varpi_B \neq 0$ one finds a stationary phase for

$$(m_1-m_2)\frac{\varpi_B L}{\overline{v}} \approx \Delta\Phi^{m_1m_2}_{\text{opt}}(\overline{v}) + \overline{v}\frac{\partial}{\partial v}\delta\varphi^{m_1m_2}_{\text{VdW}}(\overline{v},\Omega^{\text{eff}}_R). \tag{4.8}$$

For each term, there is a specific value of $\varpi_B L$ (thus of $\overline{B}$) where the envelope has a maximum, and around which fringes may be observed, as shown hereafter (classically, a number of fringes $\approx 2\overline{v}/\Delta v$, that is, ≈ 10 for a neon supersonic beam). Using a magnetic field thus allows a *compensation of the intrinsic dispersivity* of the atom mirror, as well as it provides an easy tunable parameter for the fringes scanning. Moreover, different positioning of the envelopes of the patterns contained in the signal (4.5) may be taken advantage of to isolate groups of specific fringes with a specific step.

C. Some examples of the sensitivity to van der Waals forces

It makes sense that $\Delta\Phi^{mm'}$ is more sensitive to van der Waals forces as the distance between classical turning points y_r^m and $y_r^{m'}$ is larger, that is, when the Clebsch-Gordon coefficients ξ_m and $\xi_{m'}$ differ more. Figure 4 shows this influence for two transitions: $|F_g=2,m\rangle \rightarrow |F_e=3,m\rangle$ and $|F_g=2,m\rangle \rightarrow |F_e=2,m\rangle$ (polarization π of the electric field). In the latter case, the ratio $(\xi_{m=2}/\xi_{m'=1})^2=4$, which is particularly advantageous. The number of different patterns depends of the coefficients in Eq. (4.4) standing for the preparing and analyzing steps, while their shift with $\Omega_R^{\rm eff}$ is given by $\delta\varphi_{\rm VdW}^{mm'}(\Omega_R^{\rm eff})$. We give an example of the expected signal when using the $F_g=2\rightarrow F_e=2$ transition for the atom mirror. With that transition, for which $\xi_{m=0}=0$, there is no optical potential for atoms in the $|F_g=2,m=0\rangle$ level, which are not reflected; since the phases Φ^m depend only on $|m|$, the only phase difference to be considered is then $\Delta\Phi^{2,1}$. From Eq. (4.4) the signal may be written as a sum of six terms:

$$\begin{aligned}\mathcal{S}=&A_1\cos(2\Phi_B)+A_2\cos(4\Phi_B)+A_3\cos(\Delta\Phi^{2,1}+\Phi_B)\\&+A_4\cos(\Delta\Phi^{2,1}-\Phi_B)+A_5\cos(\Delta\Phi^{2,1}+3\Phi_B)\\&+A_6\cos(\Delta\Phi^{2,1}-3\Phi_B).\end{aligned}\tag{4.9}$$

Let us focus on the last four terms, which carry information on the van der Waals interaction. Taking for simplicity's sake a Gaussian velocity distribution,

$$\rho(v_\parallel-\overline{v})\propto\exp-\left[\frac{v_\parallel-\overline{v}}{\Delta v}\right]^2,\tag{4.10}$$

it is easily shown that after integration over $v_\parallel$ each term yields a pattern whose form is given by

$$\begin{aligned}&\cos[\pm\{1,3\}\Phi_B(\overline{v})+\Delta\Phi_{\rm opt}^{2,1}(\overline{v})+\delta\varphi_{\rm VdW}^{2,1}(\overline{v},\Omega_R^{\rm eff})]\\&\times\exp-\left[\frac{\Delta v^2}{4\overline{v}^2}\left(\pm\{1,3\}\Phi_B(\overline{v})-\Delta\Phi_{\rm opt}^{2,1}(\overline{v})\right.\right.\\&\left.\left.-\overline{v}\frac{\partial}{\partial v}\delta\varphi_{\rm VdW}^{2,1}(\overline{v},\Omega_R^{\rm eff})\right)^2\right].\end{aligned}\tag{4.11}$$

When scanning $\Omega_R^{\rm eff}$, van der Waals interaction thus induces shifts both of the fringe patterns and of their respective envelopes, which are, respectively, governed by $\delta\varphi_{\rm VdW}^{2,1}(\overline{v},\Omega_R^{\rm eff})$ and $\overline{v}\partial\delta\varphi_{\rm VdW}^{2,1}(\overline{v},\Omega_R^{\rm eff})/\partial v$. Figure 5 exhibits the variations of these quantities as functions of $\Omega_R^{\rm eff}$. Since their signs are the same,[1] a specific pattern and its envelope are shifted in opposite directions versus Φ_B. Figure 6 shows that evolution for the term proportional to $\cos[-\Phi_B+\Delta\Phi_{\rm opt}^{2,1}(\overline{v})+\delta\varphi_{\rm VdW}^{2,1}(\overline{v},\Omega_R^{\rm eff})]$. An example of the total signal (4.9) is given in Fig. 7 for a specific experimental scheme (see caption).

[1]This comes easily out of the variation of the integral (3.6) as a function of the atom velocity (through E_y).

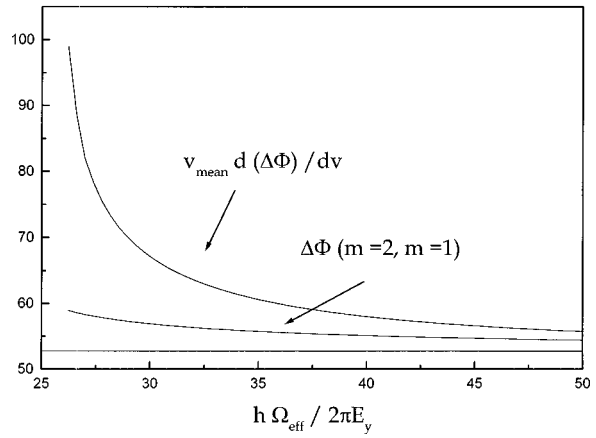

FIG. 5. van der Waals phase and shift of the fringe pattern, and of the envelope center, when scanning the Rabi frequency (see text). $(2\pi)^{-1}C_g=2$ kHz μm^3; other parameters as in Fig. 4(a). Velocity distribution $\Delta v/\overline{v}\approx 10\%$.

V. DISCUSSION AND FURTHER PROSPECTS

As seen in Fig. 4, the phases produced by the van der Waals forces are on the order of 2π, and are maximum, as expected, when the atom comes closer to the surface, that is, when the potential barrier height resulting from the competition between the van der Waals interaction and the optical potential equals the value of the total energy of the incoming atom. These phases produce sizable shifts of the fringe pattern, which are functions of the Rabi frequency, and may be fairly monitored in an experiment. The values of the van der Waals strength constant $\hbar C_g$ taken to carry out the computations shown in Fig. 4 were chosen over a range of 1–4 kHz μm^3, surrounding values obtained in studies of surface-alkali-metal systems [14]. A calculation for neon [28], taking into account the levels of the first resonant configuration $(2p_n)$ above the metastable levels, yields for level $1s^5(J=2)$ a value of $(2\pi)^{-1}C_g\cong 1.7$ kHz μm^3 for a metallic surface, which gives $(2\pi)^{-1}C_g\cong 1.1$ kHz μm^3 in the case of a dielectric material with index $n=2.2$, as often used in atom mirrors [14,18]. Comparison of our predictions to observed phases should give accurate access to experimental values of these van der Waals constants.

The present model relies on the assumption of a *scalar* van der Waals interaction. Mentioned calculations for the metastable level $1s^5$ in neon [28] exhibit a relative anisotropy of van der Waals strengths between $|g,m_y=2\rangle$ and $|g,m_y'=0\rangle$ substates (evaluated with the quantum axis along the transverse $o\vec{y}$ direction, which is the symmetry axis of the interaction) lower than 1%. In such a case, the scalar assumption, which allows for neglecting the van der Waals coupling between the paths of the interferometer in the chosen configuration, is fairly reasonable [29]. For a nonzero anisotropy, the phases accumulated in the interferometer should depend on the considered Zeeman substates, producing an additional shift of the interferometric fringes. The coupling induced between different Zeeman substates by the *off-diagonal* part of the van der Waals interaction must become effective in the case of larger anisotropies, and would result in more complex effects than phase accumulation

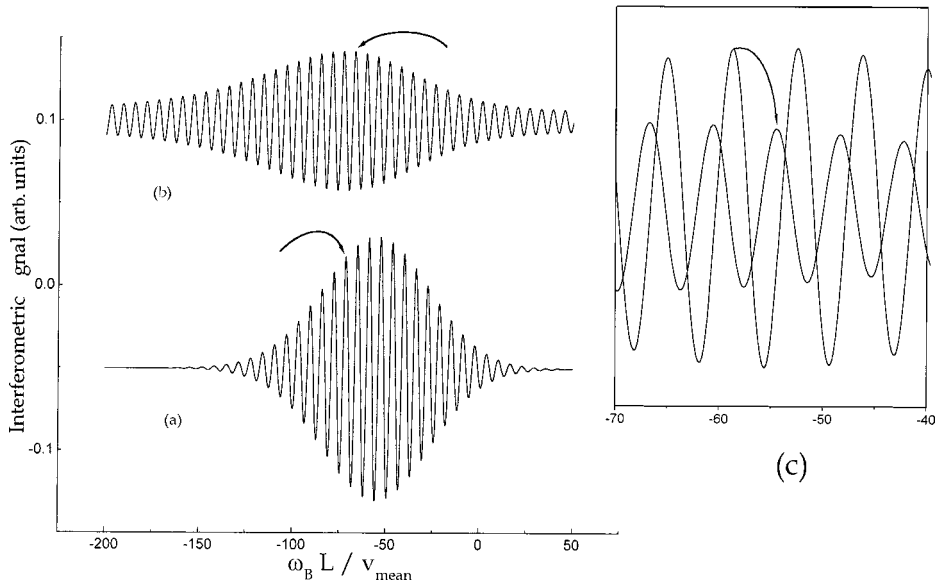

FIG. 6. Shift of the fringe patterns due to the van der Waals phase, for the transition $J=2 \leftrightarrow J=2$ at $\lambda_{opt}=614.3$ nm, when scanning down the Rabi frequency. (a) $(2\pi)^{-1}\Omega_R^2(0)/4\Delta=2.4$ GHz; (b) $(2\pi)^{-1}\Omega_R^2(0)/4\Delta=1.6$ GHz. van der Waals strength $(2\pi)^{-1}C_g=2$ kHz μm^3, other parameters as in Fig. 3. Arrows show the corresponding fringes. Velocity distribution $\Delta v/\overline{v}_{mean}\approx 8\%$. In (b), where the mean incoming energy reaches approximately the potential barrier height, part of the atoms are not reflected, which is equivalent to a narrowing of the velocity distribution, and more fringes are visible. (c) Enlargement of part of the fringe patterns.

along independent paths. For instance, a transfer between an incoming selected state $|g,m\rangle$ and a different outgoing $|g,m'\rangle$ state (with respect to our $o\overline{z}$ direction) is then possible, whose observation may be thought of in devoted experiments. The possibility of such transfers due to a van der Waals coupling between Zeeman substates belonging to two *different metastable levels* has been studied in the case of rare gases [22].

Our calculations take into account the van der Waals part of the atom-surface forces, whose variation with the transverse distance is given by $V_{VdW}=-\hbar C_g y^{-3}$. Full quantum treatments of the interaction show a discrepancy from this law at relatively large distances ($\geqslant$100 nm), referred to as the Casimir-Polder effect, which may be described *in this range* by a single potential $V_{CP}=-\hbar C_g^{CP} y^{-4}$. We have performed computations with a more general law exhibiting either van der Waals or Casimir-Polder behaviors in the appropriate limiting cases, and found no significant differences (within 3%) with respect to the sole van der Waals potential, for atom mirrors in the thermal velocity range. Departure from the van der Waals results arises, however, when considering incoming atoms with much lower energies (velocities), e.g., for a beam of laser-decelerated atoms. Optical potentials necessary to get reflection are then much lower, and the classical turning points scan larger distances from the surface, which yields an overall better sensitivity to the long-distance contribution. Sensitivity of an atom mirror threshold to the Casimir-Polder long-range contribution was discussed in studies on alkali-metal-surface systems [14], where cold atoms released from a MOT trap were considered.

In conclusion, we have given a quantitative evaluation of the *phases* brought up by van der Waals atom-surface interactions to the de Broglie wave associated to the center-of-mass motion of an atom in an atomic mirror, and proposed an atom interferometer based on polarization interferometry as a convenient scheme to measure them. It has been shown that the property of insensitivity to the evanescent wave amplitude of the phase differences due to the sole atomic mirror along the interferometer paths provides direct access to these van der Waals contributions. We have proposed merging the interferometer into a static magnetic field and analyzed its double purpose, providing a convenient scanning parameter and allowing fringe pattern observations for atoms with a longitudinal velocity distribution thanks to dispersivity com-

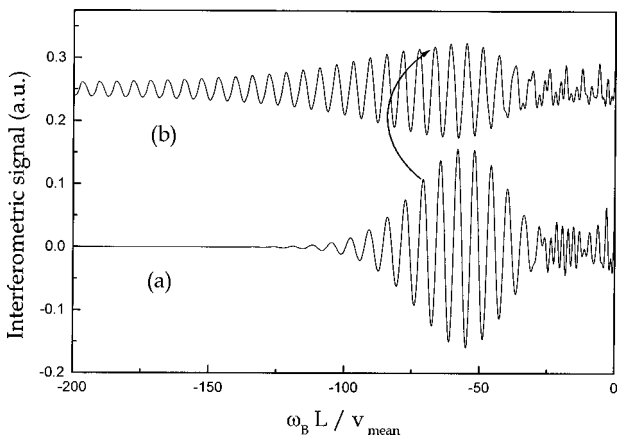

FIG. 7. An example of the expected total fringe signal [Eq. (4.9)]. Coefficients have been taken such that the mixing and analyzing zones are equivalent to a sudden rotation by 60° of the quantization axis [18,26]. Velocity distribution $\Delta v/\overline{v}_{mean}\approx 12\%$, other parameters as in Fig. 6. The main contribution comes from the term exhibited in Fig. 6.

pensation. We have predicted that the sensitivity of this type of interferometer to van der Waals interactions must be quite high, and should yield a promising alternative to the measurement of atom-surface interactions in a ground (or metastable) state by mechanical approaches.

ACKNOWLEDGMENTS

The authors would like to thank Dr. J. Baudon, Dr. Ch. Miniatura, Dr. J. Reinhardt, and Dr. J. Robert for useful discussions.

[1] J. E. Lennard-Jones, Trans. Faraday Soc. **28**, 334 (1932).
[2] H. B. G. Casimir and D. Polder, Phys. Rev. **73**, 360 (1948).
[3] E. M. Lifschitz, Zh. Eksp. Teor. Fiz. **29**, 94 (1956) [Sov. Phys. JETP **2**, 73 (1956)].
[4] S. Haroche, in *Fundamental Systems in Quantum Optics*, pp. 767–940 (North-Holland, Amsterdam, 1992); E. A. Hinds, Adv. At., Mol., Opt. Phys. Suppl. **2**, 1 (1994).
[5] K. H. Drexhage, H. Kuhn, and F. P. Schafer, Ber. Bunsenges. Phys. Chem. **72**, 329 (1968); K. H. Drexhage, Appl. Phys. Lett. **14**, 318 (1969).
[6] A. D. McLachlan, Proc. R. Soc. London, Ser. A **271**, 387 (1963); Mol. Phys. **6**, 423 (1963).
[7] E. A. Hinds and V. Sandoghdar, Phys. Rev. A **43**, 398 (1991), and references therein.
[8] R. R. Chance, A. Prock, and R. Silbey, Phys. Rev. A **12**, 1448 (1975).
[9] J. M. Wylie and J. E. Sipe, Phys. Rev. A **32**, 2030 (1985); M. Fichet, F. Schuller, D. Bloch, and M. Ducloy, *ibid.* **51**, 1553 (1995).
[10] H. Failache, S. Saltiel, M. Fichet, D. Bloch, and M. Ducloy, Phys. Rev. Lett. (to be published).
[11] D. Raskin and P. Kush, Phys. Rev. **179**, 712 (1969).
[12] A. Shih and V. A. Parsegian, Phys. Rev. A **12**, 835 (1975).
[13] A. Anderson, S. Haroche, E. A. Hinds, W. Jhe, and D. Meschede, Phys. Rev. A **37**, 3594 (1988).
[14] C. Henkel, J.-Y. Courtois, R. Kaiser, C. Westbrook, and A. Aspect, Laser Phys. **4**, 1040 (1994); A. Landragin, J.-Y. Courtois, G. Labeyrie, N. Vansteenkiste, C. I. Westbrook, and A. Aspect, Phys. Rev. Lett. **77**, 1464 (1996).
[15] M. Oria, M. Chrevrollier, D. Bloch, M. Fichet, and M. Ducloy, Europhys. Lett. **14**, 527 (1991).
[16] M. Chevrollier, M. Fichet, M. Oria, G. Rahmat, D. Bloch, and M. Ducloy, J. Phys. II **2**, 631 (1992).
[17] V. Sandoghdar, C. I. Sukenik, E. A. Hinds, and S. Haroche, Phys. Rev. Lett. **68**, 3432 (1992).
[18] S. Feron, Ph.D. thesis, Université Paris–Nord, France (1994).
[19] R. J. Cook and R. K. Hill, Opt. Commun. **43**, 258 (1982).
[20] S. Feron, J. Reinhardt, S. Le Boiteux, O. Gorceix, J. Baudon, M. Ducloy, J. Robert, Ch. Miniatura, S. Nic Chormaic, H. Haberland, and V. Lorent, Opt. Commun. **102**, 83 (1993); M. Christ, A. Scholtz, M. Schiffer, R. Deutschmann, and W. Ertmer, *ibid.* **107**, 211 (1994), and references therein.
[21] J. Baudon *et al.*, Comments At. Mol. Phys. **34**, 161 (1999), and references therein.
[22] M. Boustimi *et al.* (unpublished).
[23] See, for instance, Ch. J. Joachain, *Quantum Collision Theory* (North-Holland, Amsterdam, 1979).
[24] A. S. Dickinson, Mol. Phys. **18**, 441 (1970).
[25] Ch. J. Bordé, Phys. Lett. A **140**, 10 (1989).
[26] Ch. Miniatura, J. Robert, S. Le Boiteux, J. Reinhardt, and J. Baudon, Appl. Phys. B: Photophys. Laser Chem. **54**, 347 (1992).
[27] The relevant transverse distribution in an atomic mirror results both from the cross section for the atoms of the evanescent wave zone on the surface, typically 0.5-mm view at an angle of $\alpha_{\mathrm{in}} \approx 2$ mrad, that is, 1 μm, and from the slit in front of the detecting device, say 10 μm. At an observation distance on the order of 1 m, this gives an overall aperture of 10^{-5}, that is, with an average longitudinal velocity $\overline{v} \approx 1$ km/s, a transverse distribution $\Delta v_y \approx 10^{-2}$ m/s, and a relative transverse width $\Delta v_y / \overline{v_y} \approx 1/200$ when taking $\overline{v_y} \approx \alpha_{\mathrm{in}} \overline{v}$. The influence of this distribution in the present study may be neglected when compared to that of $\Delta v / \overline{v} \approx 1/10$ due to the longitudinal (here parallel) distribution analyzed further on.
[28] M. Ducloy (unpublished).
[29] For the ground state of alkali metals, the *s* character of the electronic wave function implies that atom-surface interactions are purely *scalar* (no quadrupolar components).
[30] M. Olshanii (private communication).